frontiers | Frontiers in Earth Science

TYPE Original Research
PUBLISHED 13 March 2023
DOI 10.3389/feart.2023.1121618

OPEN ACCESS

EDITED BY
Guangjin Wang,
Kunming University of Science and Technology, China

REVIEWED BY
Zheng Zhi,
Guangxi University, China
Rui Li,
Chongqing University, China

*CORRESPONDENCE
Jiabing Zhang,
zjb22@mails.jlu.edu.cn
Yingchun Li,
751789319@qq.com

SPECIALTY SECTION
This article was submitted to Environmental Informatics and Remote Sensing, a section of the journal Frontiers in Earth Science

RECEIVED 12 December 2022
ACCEPTED 21 February 2023
PUBLISHED 13 March 2023

CITATION
Hu N, Zhang J, Teng L, Lu Y, Li Y, Li X and Zhu C (2023), Analysis of displacement evolution characteristics of reverse-dip layered rock slope based on geological geometric partition.
Front. Earth Sci. 11:1121618.
doi: 10.3389/feart.2023.1121618

Analysis of displacement evolution characteristics of reverse-dip layered rock slope based on geological geometric partition

Nanxiang Hu[1,2,3,4], Jiabing Zhang[2,3,5]*, Lin Teng[1], Yiping Lu[4], Yingchun Li[1]*, Xiaoshuang Li[1] and Chun Zhu[1,2,3,4]

[1]College of Civil Engineering, Qilu Institute of Technology, Jinan, China, [2]Key Laboratory of Geohazard, Fujian Province, Fuzhou, China, [3]Key Laboratory of Geohazard Prevention of Hilly Mountains, Ministry of Natural Resources of China, Fuzhou, China, [4]School of Earth Science and Engineering, Hohai University, Nanjing, China, [5]College of Construction Engineering, Jilin University, Changchu, China

To investigate the toppling displacement evolution characteristics of anti-dip rock slopes, the Xiaodongcao-Zhengjiadagou bank slope is taken as an engineering case, and firstly, the geological geometric distribution characteristics of the slope are obtained by superimposing the lithology, slope, and elevation raster layers of the slope through ArcGIS, and the geological partition with the largest area is the Lower Triassic Daye Formation, bottom elevation, and medium slope; based on the actual surface displacement monitoring data, the spatio-temporal evolution nephogram of toppling displacement of bank slope every half year is interpolated by Inverse Distance Weight method, and then the last displacement nephogram is assigned to the thousandth and superimposed with the geological geometric partition to obtain the displacement superposition characteristics. The results show that: the obvious zone of horizontal displacement deformation mainly occurs in the front and middle of the bank slope, mainly shear deformation, vertical displacement is primarily in the front and the back edge of the bank slope and the total displacement deformation is more similar to the horizontal displacement; the horizontal displacement value is larger than the vertical displacement value, the horizontal displacement deformation controls the overall deformation of the bank slope; through the analysis of the geometric superposition evolution of the anti-dip rock slope, the displacement superposition strong deformation zone is located at the boundary between the Triassic Jialingjiang Formation (T1j) and the Triassic Daye Formation (T1d).

KEYWORDS

anti-dip slope, displacement nephogram, evolution characteristics, strong deformation zone, geological partition

1 Introduction

Southwest China is a region where landslide geological disasters occur frequently, and the analysis of the deformation characteristics of landslides is one of the essential aspects of landslide control (Bao et al., 2023). Especially when encountering complex geological conditions such as broken structural surface, weak interlayer and fault, the stability of landslide is greatly reduced (Wang et., 2022a; Wang et., 2022b; He et al., 2022).

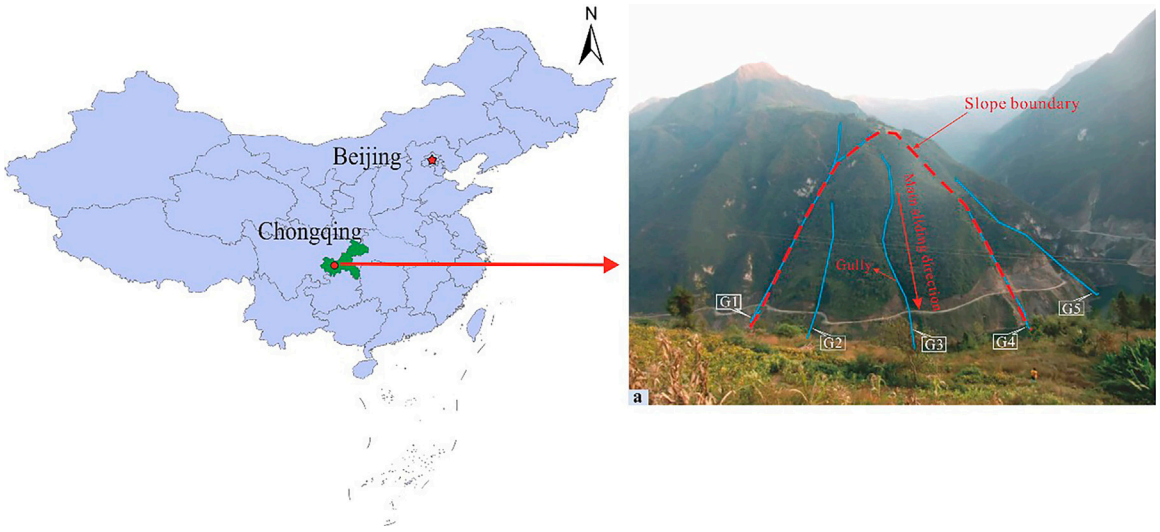

FIGURE 1
The whole landscape of the bank slope.

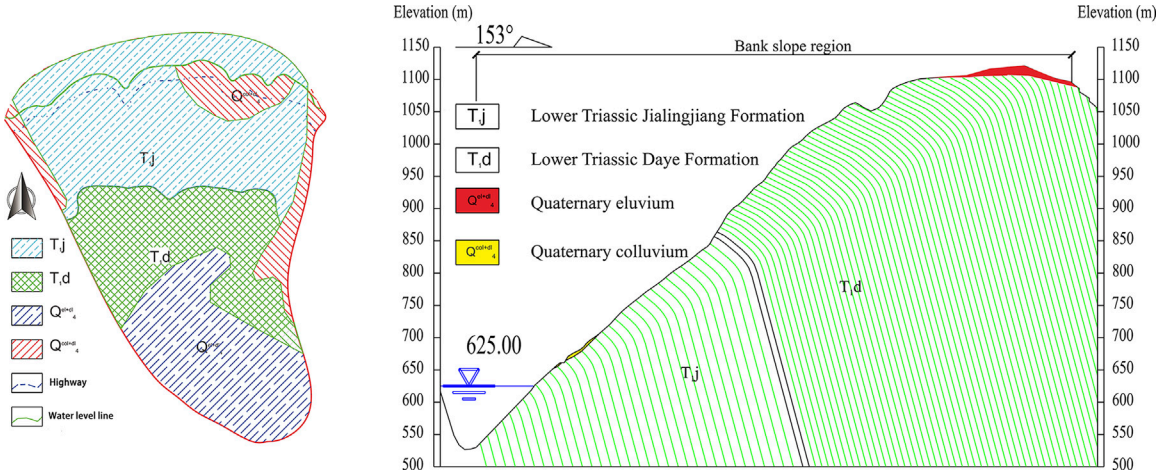

FIGURE 2
Distribution and geological section of exposed rock and soil on bank slope.

Huang. (2012) studied some typical large-scale landslides in mainland China in the 20th century and developed a geomechanical model for large-scale toppling in anti-dip strata. Goodman and Bray. (1976) classified the damage mode of anti-dip slopes into three main types: bending damage, block damage, and bending-block damage. Liu et al. (2009), Liu et al. (2010) conducted a more in-depth study on overturning damage of rock slopes based on Goodman's theory of rock slope damage. Chen et al. (2016) established a mechanical model and stability analysis method for bending and tipping damage of anti-dip rock slopes based on limit equilibrium theory. Shen et al. (2010) studied the rheological properties of red soft rock, and their results have important reference values for the design of anti-dip red soft rock slopes. Adhikary et al. (1997) conducted a series of model centrifugal tests to study the bending and tipping damage mechanism of jointed rock slopes. Alejano et al. (2010) used numerical analysis to analyze the damage mechanism of open pit mine. They interpreted the anti-dip stratified slope as a complex combination of tipping and cyclic damage. Bowa and Xia. (2018) proposed a technique for angular analysis of counter-tilted failure surfaces applicable to block tipping failure mechanisms, which can provide an accurate application for evaluating the instability of rock slopes with counter-tilted failure surfaces. Li et al. (2019) analyzed the width, and ridge number variation characteristics of the fast Fourier transform spectrum along the slope surface to reveal the internal damage characteristics of anti-dip rock slopes. Ning et al. (2019) conducted a simulation study on the evolutionary characteristics of toppling failure of anti-dip rock slopes and revealed the relationships between the surface peak ground

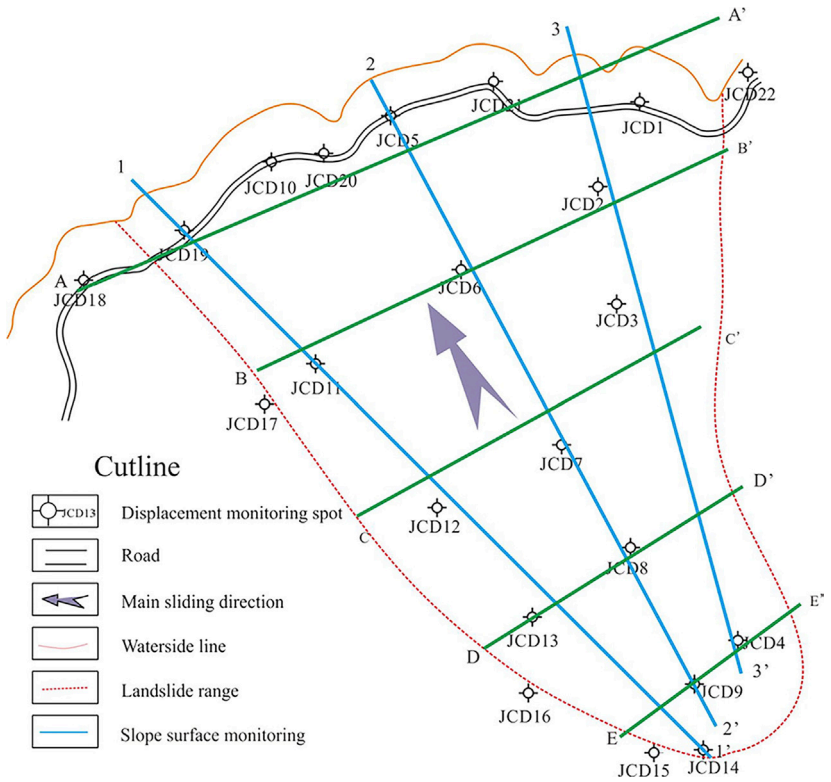

FIGURE 3
Plane layout of surface displacement monitoring.

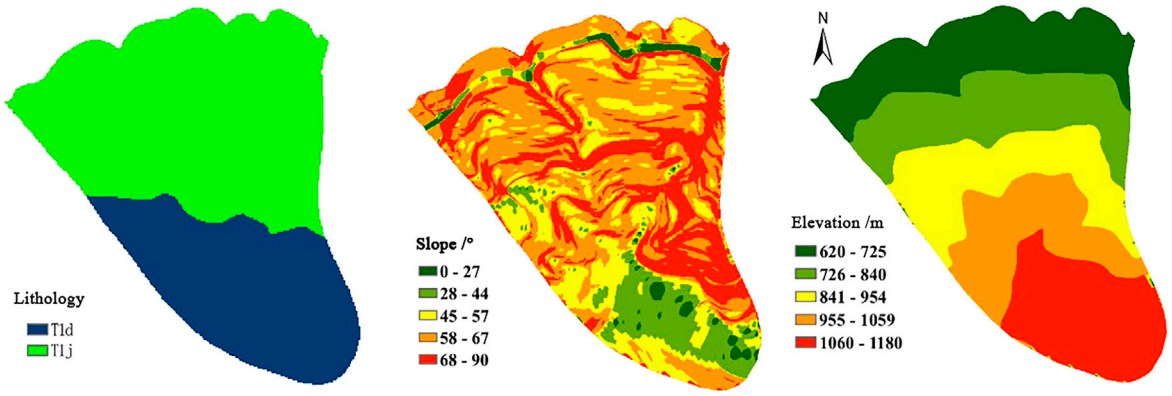

FIGURE 4
Lithology, slope, and elevation distribution map.

acceleration, the horizontal depth of the failure plane, and slope displacement. Tao et al. (2019) used the superimposed cantilever beam theory and the maximum tensile stress strength criterion for brittle damage to derive a formula for calculating the vertical crack extension depth in reverse slope overturning damage by studying and analyzing the unstable damage mode of massive overturning damage of the southwest slope of the Changshanhao open-pit gold mine. Based on the similarity ratio theory, Zhu et al. (2020) developed a physical model to investigate in depth the damage mechanism of anti-dip layered slopes during excavation. Weng et al. (2020) proposed an innovative failure criterion for assessing the stability of anti-dip rock slopes, which outperforms the Mohr-Coulomb criterion at low normal stresses and is more relevant to reality. Xie et al. (2020) analyzed the evolution characteristics of toppling deformation of rock slopes from the perspective of the energy field. Dong et al. (2020); Dong et al. (2022) combined field

TABLE 1 Bank slope geological zoning basis.

Type	Lithology	Slope/°	Elevation/m
Grade	1: Lower Triassic Daye Formation (*T1d*)	1: 0–27	1: 620–725
	2: Lower Triassic Jialingjiang Formation (*T1j*)	2:28–44	2: 726–840
		3:45–57	3: 841–954
		4:58–67	4: 955–1,059
		5: 68–90	5: 1,060–1,180
Partition number	Hundreds digit	Tens digit	Single digit

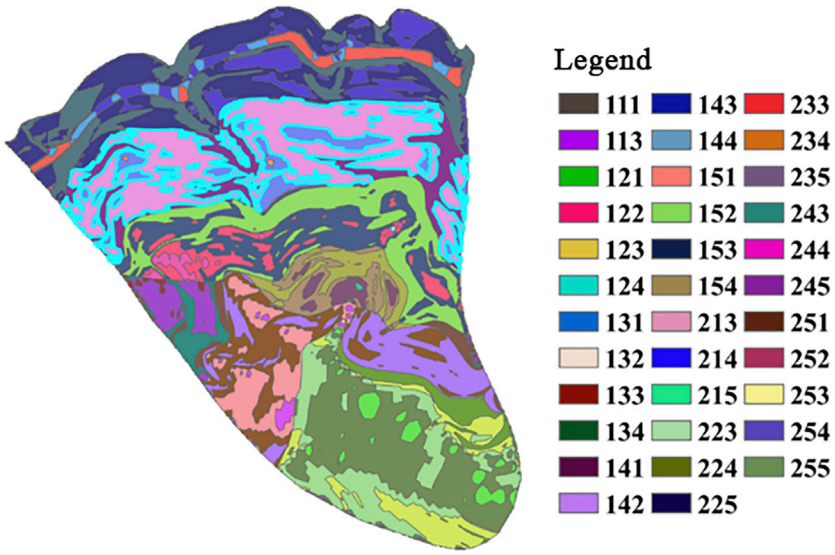

FIGURE 5
Geologic geometric displacement superimposed partition map.

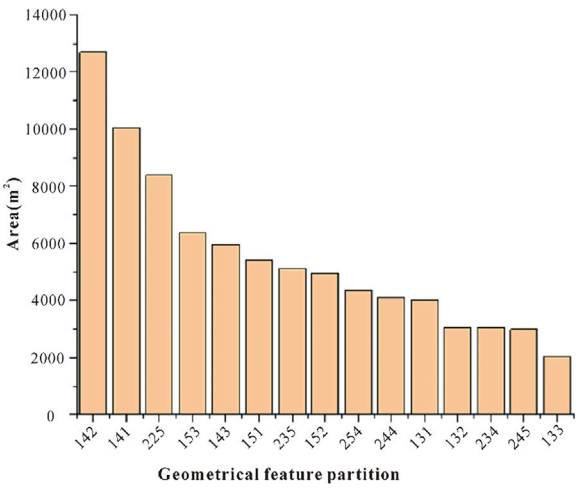

FIGURE 6
Bank slope geological geometric partitioning unit area of statistical results.

monitoring data to simulate the excavation process of anti-dip rock slopes with the discrete element method and analyzed the influence of different factors on the slope. The results show that the scale and stability of the deformation zone of the anti-dip rock slope have a specific influence, and the lithology determines the failure mode of the toppling failure. Cheng et al. (2021) used a digital camera to take high-speed images of real-time deformation behavior of overturn-resistant rock slopes under external loads, analyzed the entire damage process of anti-dip rock slopes, and discussed in detail the ultimate damage modes of the anti-dip rock slopes with different joint angles. Ding et al. (2021) studied the characteristics and process of the flexural toppling of anti-dip rock slopes. They obtained the characteristics and mechanical mechanism of flexural toppling, as well as the zoning of the slope. Xu et al. (2022) used the discrete element method (DEM) to explore the failure of earthquake-induced large-scale anti-dip rock landslides. Ren et al. (2022) used the three-dimensional discrete element method to analyze the dynamic response to the seismic dynamic of the anti-dip rock slopes. Nie et al. (2022)

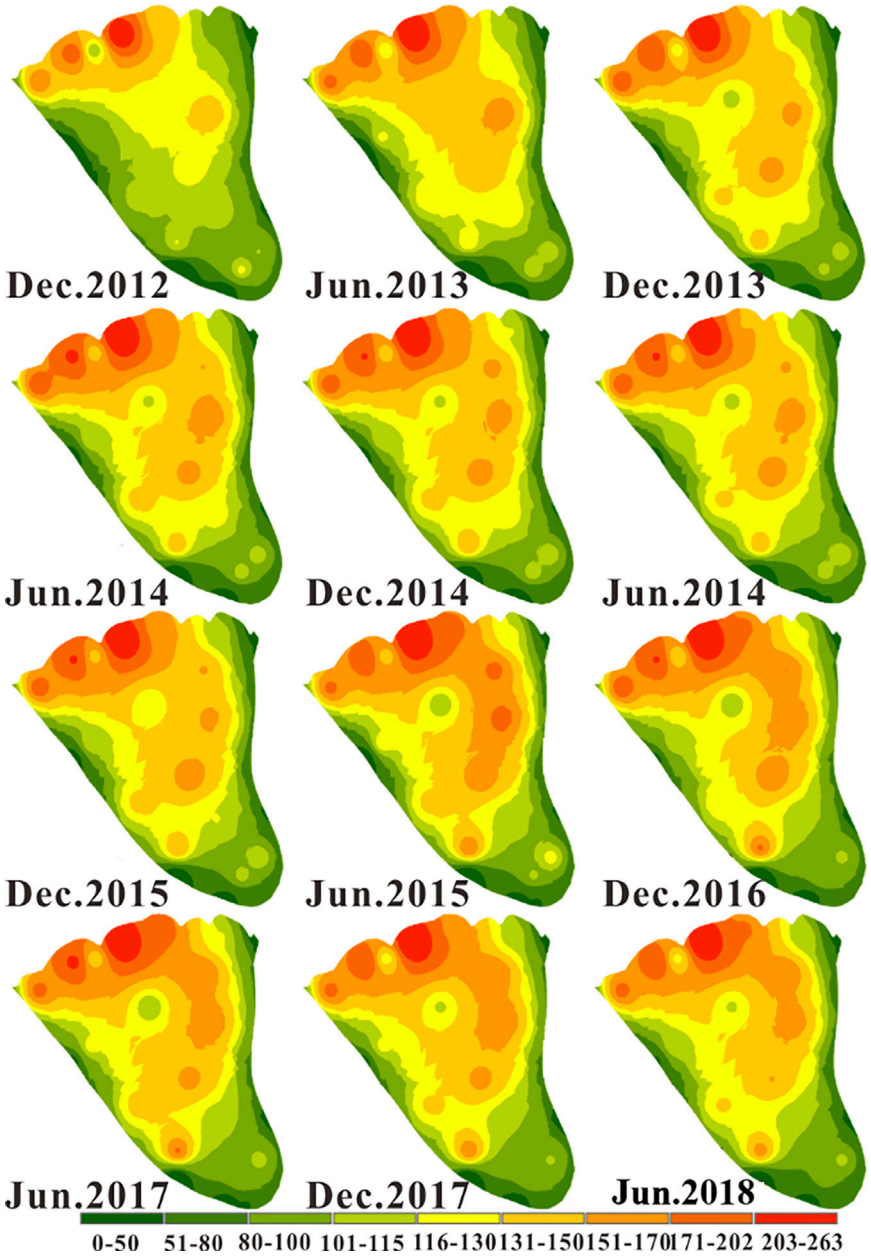

FIGURE 7
Spatial and temporal evolution nephogram of horizontal displacement (mm).

conducted a study on the control of deformation damage of NPR structural cables on rocky slopes under excavation by using numerical simulation method, and revealed the control mechanism of NPR structural cables on rocky slope tipping deformation. They studied the amplification effect, the change in the Fourier spectrum, the failure mechanism, and the permanent displacement of the slopes under seismic action.

As this project is a typical anti-dip layered rock slope, it has attracted the attention of many experts and scholars. Cai et al. (2014) established the cantilever beam limit equilibrium calculation model and verified its correctness with the numerical software UDEC, and obtained that the damage zone of anti-dip stratified rock slope is determined by the foot of the slope, dip angle of the rock layer, and slope height. Gao et al. (2015) considered the Goodman-Bray method of calculating the stability of anti-dip rock slopes under the action of groundwater. Wei. (2015) used numerical software (UDEC) to study the variation rule of toppling deformation of anti-dip slopes with the thickness ratio of adjacent rock strata. Jiang et al. (2016) divided the damage of anti-dip rock slopes into three main stages: bending, bending cracking, and fracture cracking.

Many factors affect the tipping deformation of rocky slopes, and the research results also have specific reference values. Most scholars

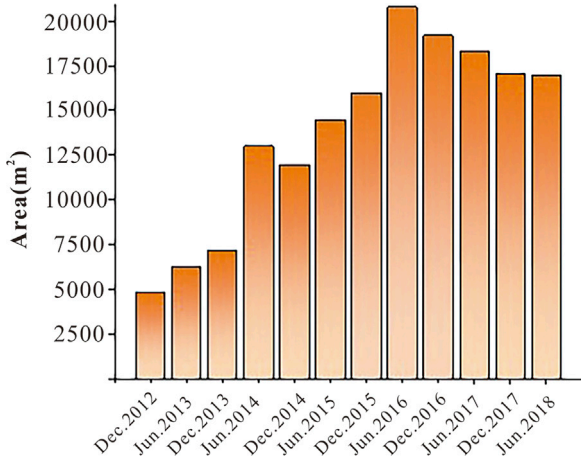

FIGURE 8
Area of horizontal displacement strong deformation zone.

mainly analyze the overall stability of anti-dip rock slopes through theoretical analysis, physical model tests, and numerical simulation, and analyze the deformation evolution characteristics of rocky slopes as a whole (Gschwind et al., 2019; Martino et al., 2020; Wang et al., 2020; Tang et al., 2022; Liang et al., 2022; Zheng et al., 2022; Lei et al., 2022; Wang et al., 2020; Wang et al., 2023; Ren et al., 2023). However, the actual monitoring data show that the deformation evolution characteristics of anti-dip rock slopes vary significantly in different areas and have different geological geometric characteristics. Therefore, this paper takes the typical anti-dip rock slope as the research object. Based on field investigation, it takes the lithology, slope, and elevation of the rock slope as the characteristic geological factors and analyzes its spatial distribution characteristics (Wang et al., 2022; Wu et al., 2022). Based on the discrete actual displacement monitoring data, the evolution nephogram of toppling displacement of rock slope is obtained by Inverse Distance Weight method, and the Spatiotemporal evolution nephogram of displacement is superimposed with geological and geometric characteristics. This study explores the geometric characteristics of the anti-dip rock slope and its displacement superposition evolution characteristics, which can provide a reference for similar engineering examples.

2 Project overview

Xiaodongcao-Zhengjiadagou bank slope is located on the right bank of the upper reaches of Xixi River, Zhongliang Township, Wuxi County, Chongqing (Figure 1), 1.2 km from Zhongliang Reservoir (Figure 1), with the elevation of the bank slope ranging from 540 m to 1,183 m and the width of 700 m; the overall topography of the bank slope is steep, the slope aspect is 345°, the vegetation in the area is developed, the front part of the topography is steep, the topography slope angle is 45°–68°, and the back part of the topography is relatively gentle, the topography slope angle is 11°–18°, and the local section can reach 37°. The topographic characteristics of the bank slope are mainly controlled by lithology and geological structure. According to the field geological survey and engineering investigation, it is revealed that the rock mass of the bank slope is mainly composed of the Lower Triassic Jialingjiang Formation (T1j) and Daye Formation (T1d); among them, Jialingjiang Formation (T1j) is a medium-thick laminated dolomitic tuff, mainly distributed in the middle and front part of the bank slope, mainly subject to shear stress. The rock structure is relatively complete, but the local weathering is substantial. The Daye Formation (T1d) is a thin and medium-thick laminated marl tuff, mainly distributed in the middle and posterior part of the bank slope, which is in the area of obvious tensile stress during the bending and tipping deformation, so the rock structure is broken, and the bending and tipping deformation of the rock layer is obvious (Figure 2).

The surface displacement monitoring system mainly consists of 22 surface displacement monitoring points evenly distributed throughout the study area, including 17 monitoring points on the bank slope body and five outside the bank slope boundary; the surface displacement monitoring time was from December 2012 to December 2016. The monitoring system was divided into five transverse and three longitudinal profiles based on their arrangement characteristics. After the reservoir completion, the water level was raised by nearly 100 m compared with the original, and the deformation of the front and trailing edge of the bank slope was more pronounced. The surface of the trailing edge showed obvious pulling cracks, which seriously threatened the life safety of the downstream residents (Figure 3).

3 Analysis of bank geometric characteristics zoning

3.1 Analysis of geometric characteristics factor

The geometric characteristics of the bank slope area were analyzed by ArcGIS, and the distribution characteristics of stratigraphic lithology, slope, and elevation in the bank slope area were obtained. As can be seen from Figure 4, the front part of the bank slope is steep, except for the rear part, which is relatively gentle (0°–27°); most of the other areas have a slope angle greater than 44°, the slope body gully is developed, the gully is “V"-shaped, with significant differences in topographic relief. The Lower Triassic Jialingjiang Formation (T1j) is located in the front to the middle of the bank slope, and the Daye Formation (T1d) is located at the rear edge of the bank slope.

3.2 Geometric characteristics superposition

The lithology, slope, and elevation raster layers were reclassified, and the lithology was assigned to the hundreds digit, slope to the tens digit, and elevation to the single digit by the Spatial Analyst tool of GIS. The geological geometry of the bank slope was performed according to the Jenks Natural Breaks Classification (Table 1), and the bank slope was finally divided into 35 characteristic partitions (Figure 5).

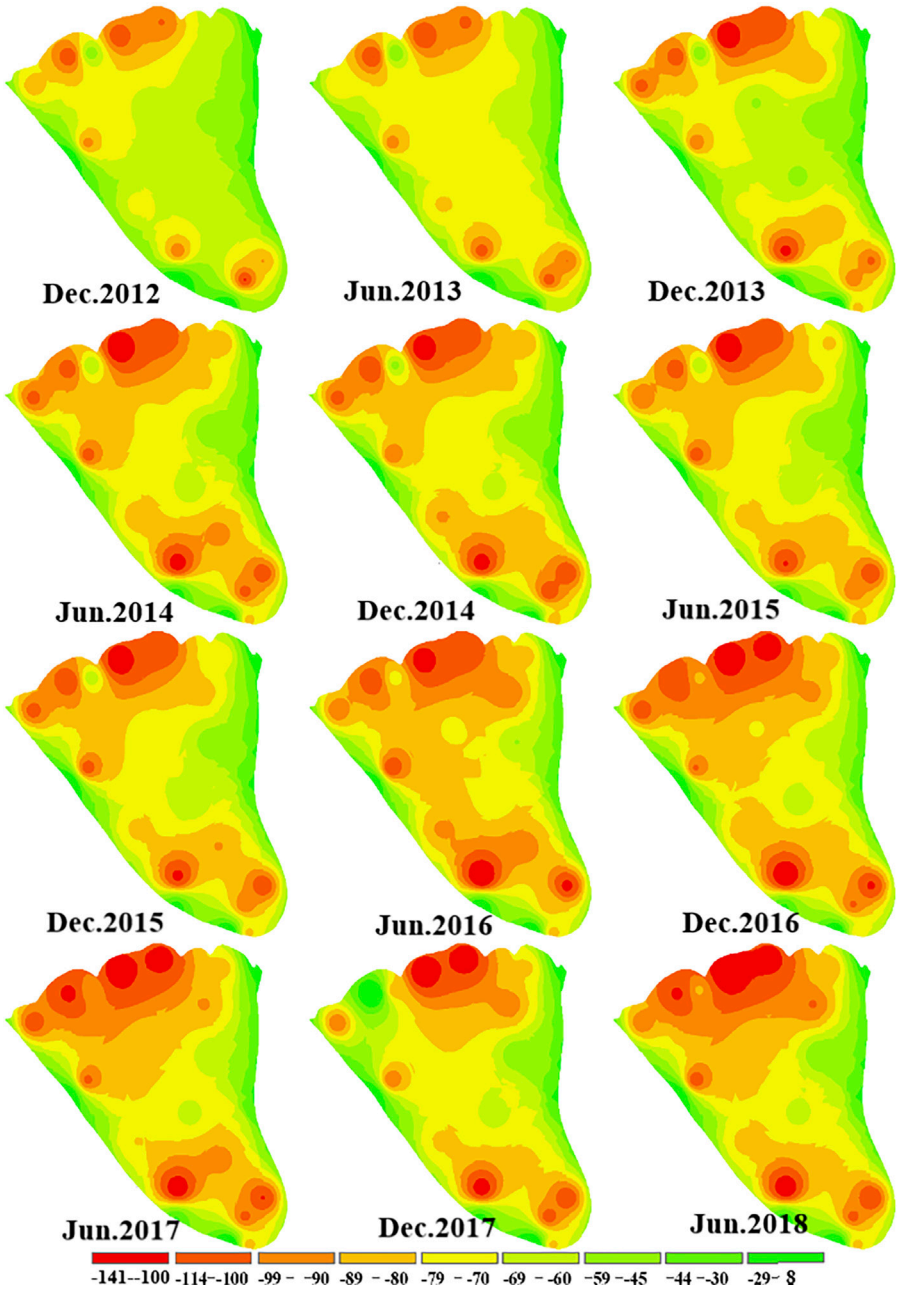

FIGURE 9
Spatial and temporal evolution nephogram of vertical displacement.

3.3 Analysis of geometric superposition characteristics

The geological geometric displacement superposition partition map can be divided into 35 characteristic partitions by GIS raster calculation, with a total area of 97039.01 m^2. Among them, the characteristic partition area with an area greater than 2000 m^2 accounts for 85.04% of the total area, and the largest characteristics partition is the 142nd (Figure 6).

4 Analysis of the evolutionary characteristics of displacement nephogram

The Inverse Distance Weight method was used to interpolate the displacement deformations of the bank slope surface monitoring points. The displacements were classified into nine categories by the Jenks Natural Breaks Classification. The horizontal displacement deformation nephogram, vertical displacement deformation nephogram, and total displacement deformation nephogram were interpolated every 6 months.

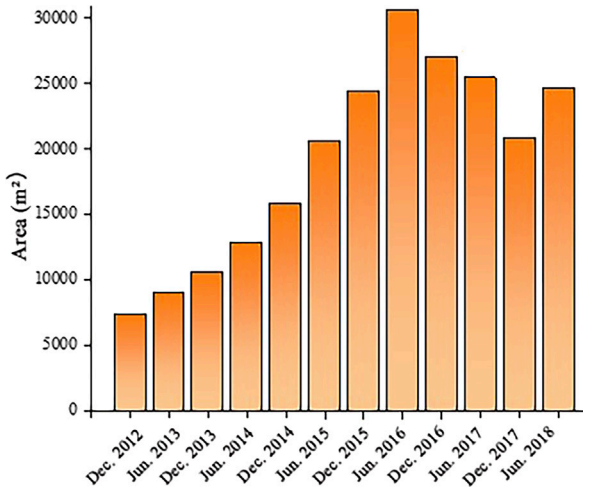

FIGURE 10
Area of strong deformation zone in the vertical direction.

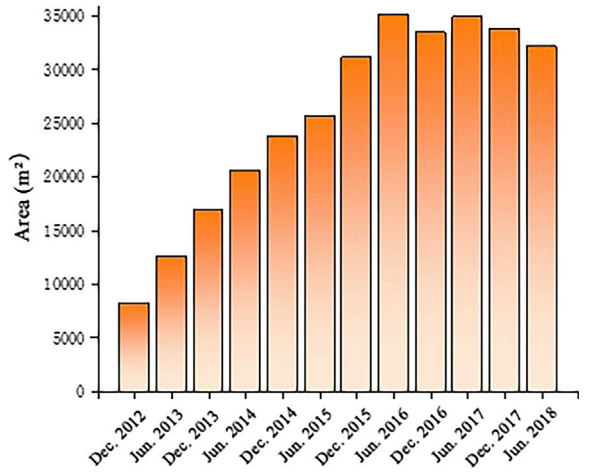

FIGURE 11
Spatial and temporal evolution nephogram of total displacement.

4.1 Analysis of the evolution of horizontal displacement nephogram

The temporal and spatial evolution nephogram of the horizontal displacement of the bank slope below (Figure 7) shows that the bank slope's obvious area of horizontal displacement deformation mainly appears in the front and middle of the bank slope. The maximum horizontal displacement appears in the front of the bank slope, mainly distributed in a dotted shape and a strip distribution in the middle. With time, it can be seen from the evolution nephogram that the horizontal displacement deformation in the middle increases significantly and gradually expands to the right side, and the horizontal displacement on the right side of the middle is significantly larger than that on the left side. The area with horizontal displacement deformation greater than 150 mm is the obvious area of horizontal displacement deformation. As shown in Figure 8, the obvious area of horizontal displacement deformation increases and decreases with time, reaching a maximum of 20780.38 m^2 in June 2016, and then the deformation of the middle displacement gradually weakens and changes to the right side of the front, gradually fading to point. The horizontal displacement of the middle strip deformation area and the front point deformation area alternately control the evolutionary law of tipping deformation of the anti-dip rock slope, where shear deformation mainly occurs.

4.2 Analysis of the evolution of vertical displacement nephogram

The temporal and spatial evolution nephogram of the vertical displacement of the bank slope below (Figure 9) shows that the obvious area of vertical displacement deformation mainly occurs in the front of the bank slope and the back edge of the bank slope. The maximum vertical displacement occurs in the middle area of the front of the bank slope and the trailing edge of the bank slope and is dotted. The vertical displacement change in the middle of the bank slope is the smallest. With time, the deformation of the front and back edges became more pronounced and gradually increased. The trailing edge of the bank slope mainly occurs in vertical deformation, corresponding to the evolution law of toppling deformation.

The vertical displacement of the front of the bank slope gradually increases overall. It gradually expands from the middle to the left and right sides, and the front middle of the bank slope and the change of vertical displacement on the left side is more evident than on the right side. The change of vertical displacement in the middle and rear part of the bank slope and the rear edge is more pronounced, with a point-like distribution, and gradually increases with time. The area with vertical displacement less than −80 mm is defined as the obvious area of vertical displacement deformation (Figure 10). In June 2016, the area of the strong deformation zone reached a maximum of 30592.39 m^2. The evolutionary characteristics of the vertical displacement in the middle of the bank slope were not prominent, and the change in the right side of the middle was small; it showed the anti-dip evolutionary characteristics of the bank slope.

4.3 Analysis of the evolution of the total displacement nephogram

The temporal and spatial evolution nephogram of the total displacement of the bank slope below (Figure 11) shows that the total displacement and horizontal displacement deformation are relatively similar, with the maximum total displacement mainly occurring in the front of the bank slope, with a point-like distribution. With time, the total displacement deformation in the middle gradually increases. As can be seen from Figure 12, the area of the total displacement strong deformation zone reached a maximum of 35057.62553 m^2 in June 2016 and expanded from the front to the middle of the bank slope, and the deformation of the right side of the middle was significantly more significant than the left side; the tipping deformation was dominated by horizontal displacement changes, and the horizontal displacement deformation was significantly more significant than the vertical displacement changes.

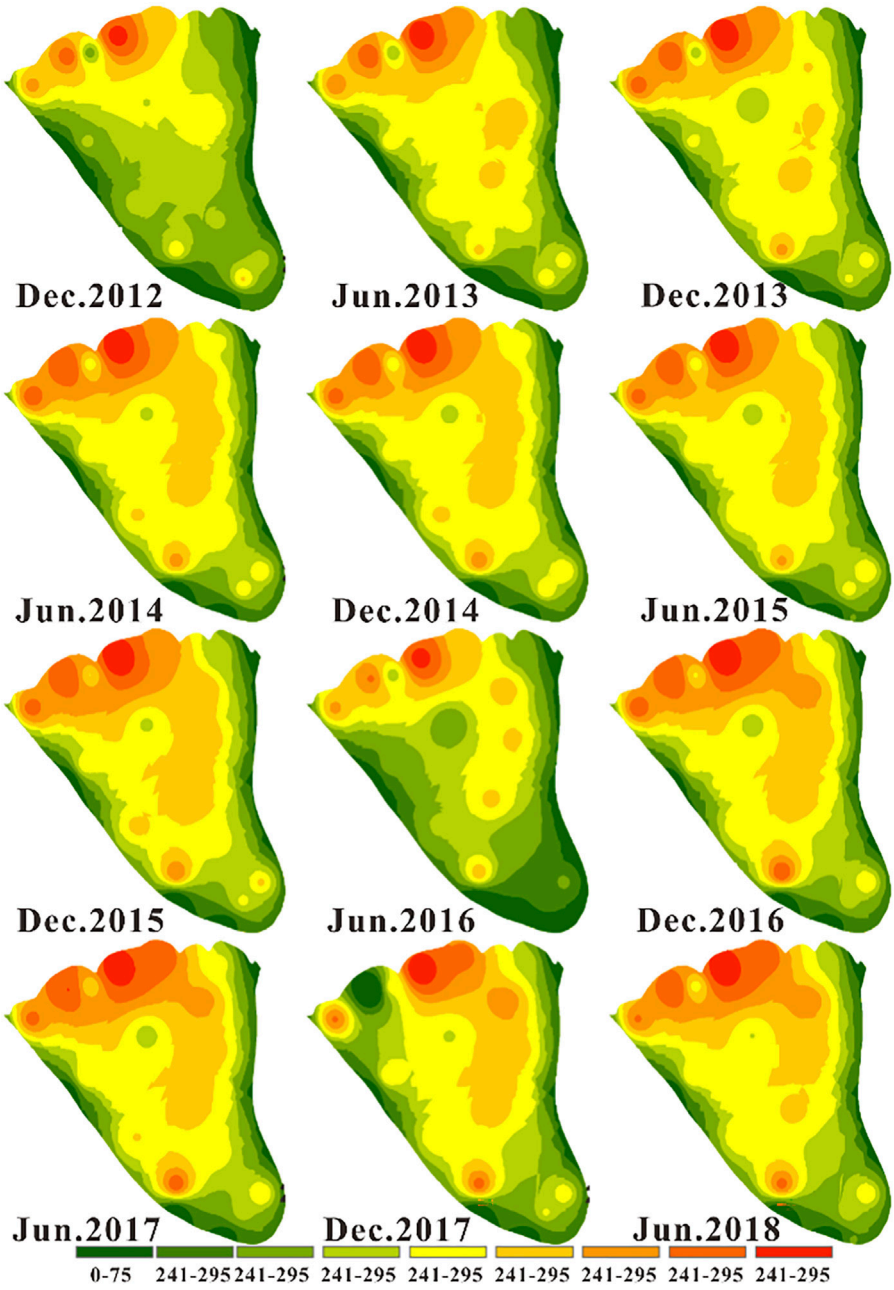

FIGURE 12
Area of strong deformation zone in total direction.

5 Analysis of displacement superposition characteristics

Based on geological geometric superposition, the horizontal displacement nephogram, vertical displacement nephogram, and total displacement nephogram of the later interpolation are assigned to the thousands digit, and the displacement geometric superposition characteristics partition based on the geological geometric partition is obtained. The displacement strong deformation zone and the most prone area of the bank slope are analyzed.

5.1 Analysis of geometric superposition characteristics of horizontal displacement

The horizontal displacement is reclassified into three categories 17 mm–103 mm as the weak deformation zone, 104–146 mm as the medium deformation zone, 147 mm–255 mm as the strong deformation zone, and the horizontal displacement is superimposed with geological geometry to get the horizontal displacement geometry superimposed characteristics zone, which is divided into 88 characteristics partitions (Figure 13).

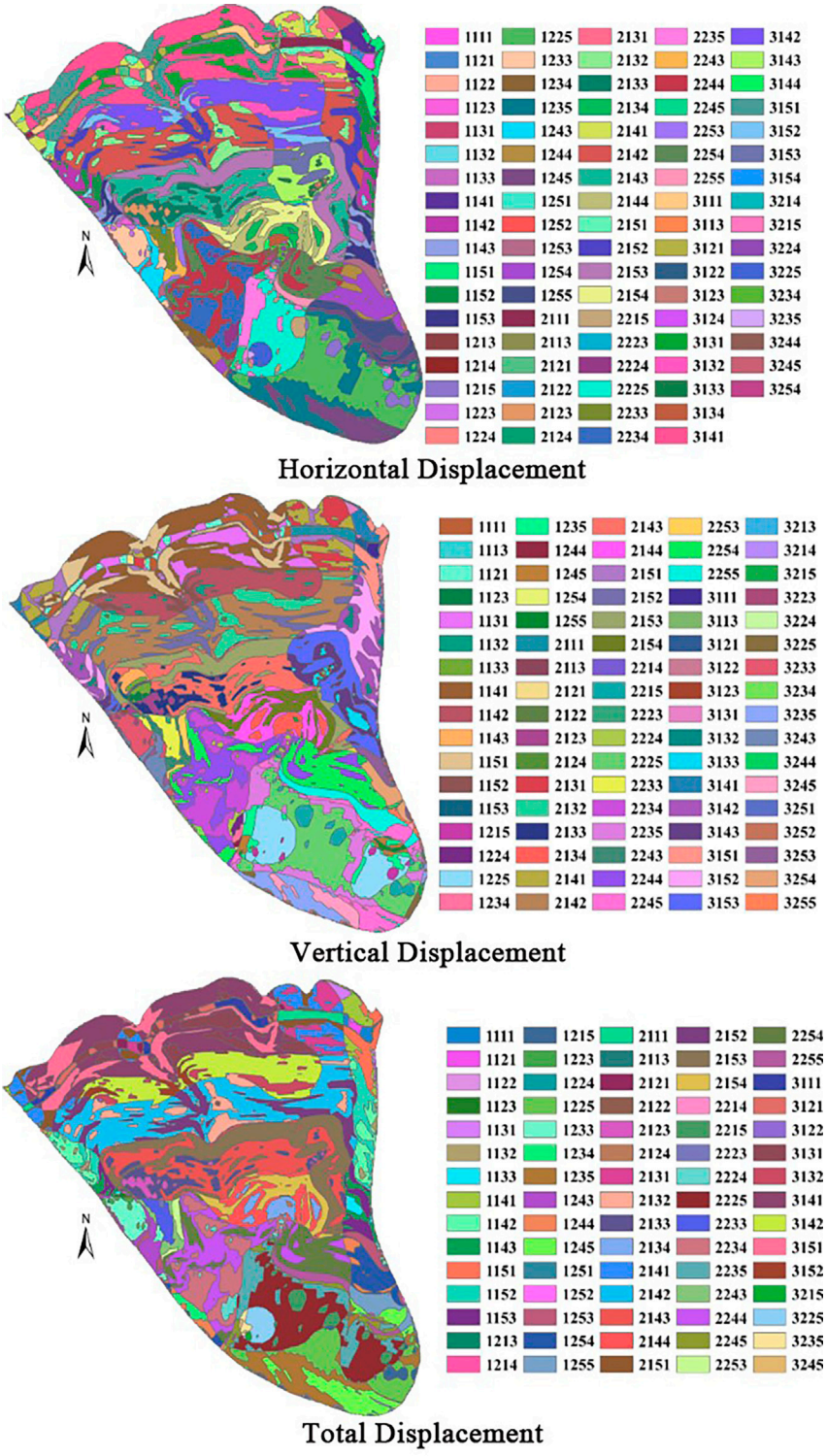

FIGURE 13
Superposition of displacement geometric characteristics.

The area of each horizontal displacement geometric superposition characteristics partition was counted by GIS (Figure 14). The characteristics partition with a strong deformation area larger than 1,500 m^2 was selected as the horizontal displacement strong deformation partition. Among them, the horizontal displacement strong deformation partition with the largest strong deformation area is the 141th partition, whose strong deformation area is 7,311.724 m^2, accounting for

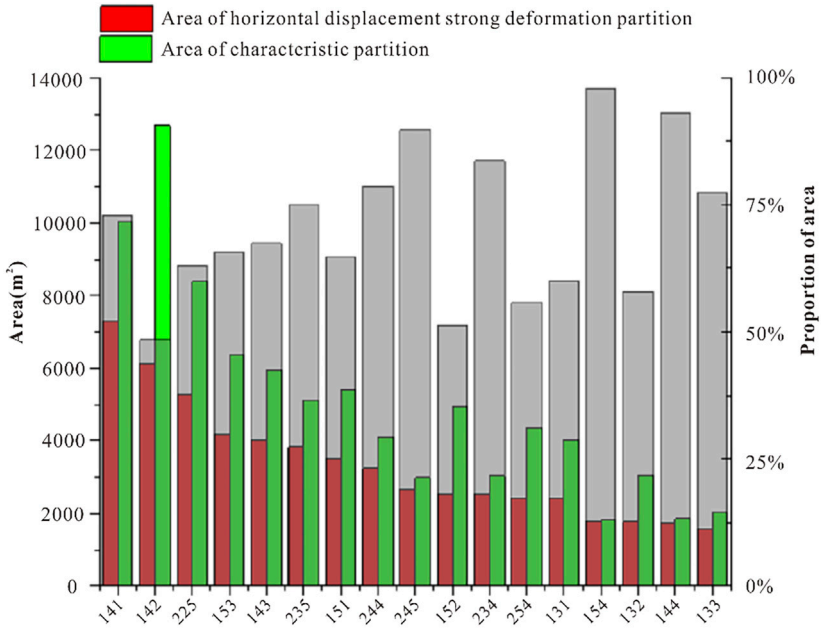

FIGURE 14
The ratio of the area of strong deformation of horizontal displacement and its characteristic area.

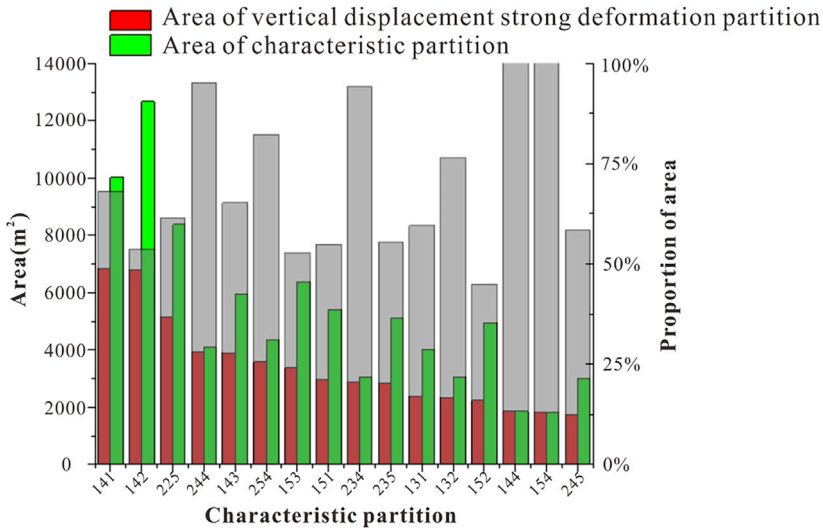

FIGURE 15
The ratio of the area of strong deformation of vertical displacement and its characteristic area.

72.29% of the 141th partition. This characteristic partition is located in the Jialingjiang Formation (T1j), medium slope, and bottom elevation. The horizontal displacement-prone partition is the 154th partition, 97.95% of which is the strong deformation zone, and the strong deformation area is 1779.01 m^2. This characteristic partition is located at the boundary between Jialingjiang Formation (T1j) and Daye Formation (T1d), high slope and medium elevation.

5.2 Analysis of geometric superposition characteristics of vertical displacement

The area of each vertical displacement geometric superposition characteristics partition was counted by GIS (Figure 15). The characteristics partition with a strong deformation area larger than 1,500 m^2 was selected as the vertical displacement strong deformation partition. Among them, the vertical displacement strong deformation

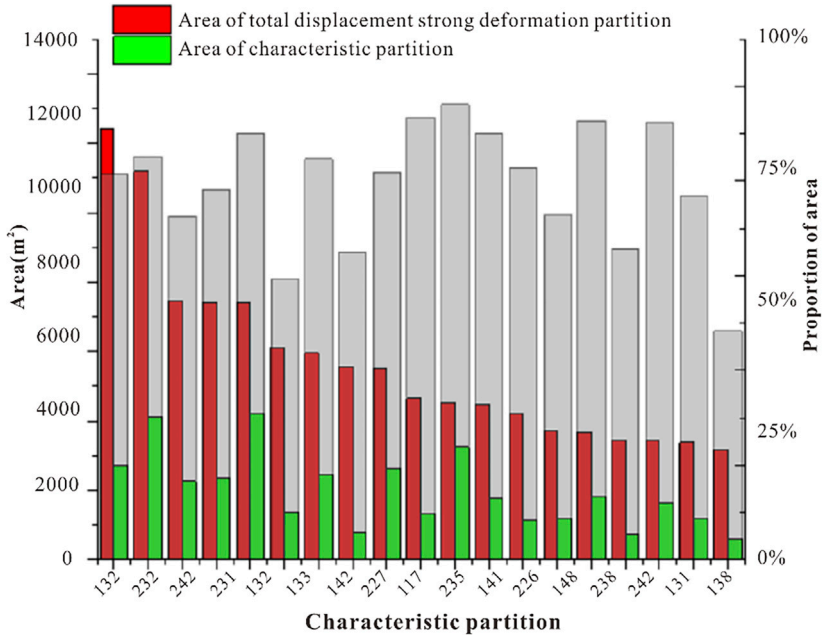

FIGURE 16
The ratio of the area of strong deformation of total displacement and its characteristic area.

partition with the largest strong deformation area is the 141th partition, whose strong deformation area is 6,832.61 m^2, accounting for 68.16% of the 141th partition. This characteristic partition is located in the Jialingjiang Formation (T1j), medium slope, and bottom elevation. The vertical displacement-prone partitions are the 154th and 14fourth, 100% of which are strong deformation zones. They are located at the boundary between Jialingjiang Formation (T1j) and Daye Formation (T1d), with a high slope and medium elevation.

5.3 Analysis of geometric superposition characteristics of total displacement

The area of each total displacement geometric superposition characteristics partition was counted by GIS (Figure 16). The characteristics partition with a strong deformation area larger than 1,500 m^2 was selected as the total displacement strong deformation partition. Among them, the total displacement strong deformation partition with the largest strong deformation area is the 132nd partition, whose strong deformation area is 6,832.61 m^2, accounting for 81.61% of the 132nd partition. This characteristic partition is located in the Jialingjiang Formation (T1j), medium slope, and bottom elevation. The total displacement-prone partition is the 235th partition, 96.21% of which is the strong deformation zone. This characteristic partition is located at the boundary between Jialingjiang Formation (T1j) and Daye Formation (T1d), high slope and medium elevation.

6 Conclusion

Based on the analysis of typical anti-dip layered rock slope cases, based on discrete surface displacement monitoring data and combined with different geological zones, this paper explores the real evolution law of toppling deformation in each zone. It can reference similar anti-dip slope monitoring, early warning, and prevention. The main results are as follows.

(1) The geometric characteristics overlay was obtained by superimposing geometric factors such as lithology, slope, and elevation of the bank slope strata through ArcGIS raster calculation. It was divided into 35 characteristics partitions with an area of 97039.01 m^2. The characteristics partition with the largest superimposed area is the 142nd partition, located in the Lower Triassic Daye Formation, bottom elevation, medium slope.
(2) The analysis of evolution characteristics of horizontal displacement nephogram, vertical displacement nephogram, and total displacement nephogram shows that the obvious zone of horizontal displacement deformation mainly occurs in the front and middle of the bank slope and is dominated by shear deformation, the vertical displacement is mainly in the front of the bank slope and the back edge, the total displacement deformation is more similar to the horizontal displacement, the horizontal displacement value is larger than the vertical displacement value, and the horizontal displacement deformation controls the overall toppling deformation of the bank slope.
(3) Based on the geological geometric superposition, the displacement nephogram of the last interpolation is overlaid with it. The results show that: the strong deformation partition of horizontal and vertical displacement is the 141th partition, and the strong deformation zone of total displacement is the 132nd partition. The horizontal displacement-prone area is the 154th partition, the vertical displacement-prone area is the

154th and fourth partition, and the total displacement-prone area is the 235 partition.

Data availability statement

The original contributions presented in the study are included in the article/supplementary material, further inquiries can be directed to the corresponding authors.

Author contributions

JZ and NH participated in the design of this study, and they both performed the statistical analysis. NH carried out the study and collected important background information. YLi drafted the manuscript. All authors read and approved the final manuscript. JZ and LT carried out the concepts, design, definition of intellectual content, literature search, data acquisition, data analysis and manuscript preparation. YLu, XL and CZ provided assistance for data acquisition, data analysis and statistical analysis. JZ and YLi carried out literature search, data acquisition and manuscript editing. XL and CZ performed manuscript review. All authors have read and approved the content of the manuscript. All authors have made substantial contributions to all of the following: (1) The conception and design of the study, or acquisition of data, or analysis and interpretation of data, (2) drafting the article or revising it critically for intellectual content, (3) final approval of the version to be submitted.

Funding

This study was supported by the Young creative talents introduction and culturing program of universities in Shandong Province (Grant No. [2021]51), the National Natural Science Foundation of Shandong Province of China (NSFC) (Grant No. ZR2022ME188), the project of Slope safety control and disaster prevention technology innovation team of "Youth Innovation Talent Introduction and Education Plan" of Shandong Colleges and universities (Grant No. Lu Jiao Ke Han [2021] No. 51), and the opening fund of Key Laboratory of Geohazard Prevention of Hilly Mountains, Ministry of Natural Resources (Grant No. FJKLGH2023K001).

Conflict of interest

The authors declare that the research was conducted in the absence of any commercial or financial relationships that could be construed as a potential conflict of interest.

Publisher's note

All claims expressed in this article are solely those of the authors and do not necessarily represent those of their affiliated organizations, or those of the publisher, the editors and the reviewers. Any product that may be evaluated in this article, or claim that may be made by its manufacturer, is not guaranteed or endorsed by the publisher.

References

Adhikary, D. P., Dyskin, A. V., Jewell, R. J., and Stewart, D. P. (1997). A study of the mechanism of flexural toppling failure of rock slopes. *Rock Mech. Rock Eng.* 30 (2), 75–93. doi:10.1007/bf01020126

Alejano, L. R., Gomez-Marquez, I., and Martinez-Alegria, R. (2010). Analysis of a complex toppling-circular slope failure. *Eng. Geol.* 114 (1-2), 93–104. doi:10.1016/j.enggeo.2010.03.005

Bao, Y. D., Chen, J. P., Su, L. J., Zhang, W., and Zhan, J. W. (2023). A novel numerical approach for rock slide blocking river based on the cefdem model: A case study from the samaoding paleolandslide blocking river event. *Eng. Geol.* 312, 106949. doi:10.1016/j.enggeo.2022.106949

Bowa, V. M., and Xia, Y. Y. (2018). Stability analyses of jointed rock slopes with counter-tilted failure surface subjected to block toppling failure mechanisms. *Arabian J. Sci. Eng.* 43 (10), 5315–5331. doi:10.1007/s13369-018-3168-4

Cai, J. S., Yan, E. C., Wang, Z. Q., Yang, J. G., and Tang, R. X. (2014). Study of cantilever beam limit equilibrium model of anti-dip layered rock slopes. *Rock Soil Mech.* 35 (S1), 15–18. doi:10.16285/j.rsm.2014.s1.003

Chen, C., Zheng, Y., and Sun, C. (2016). An analytical approach on flexural toppling failure of counter-tilt slopes of layered rock. *Chin. J. Rock Mech. Eng.* 35 (11), 2174–2187. doi:10.13722/j.cnki.jrme.2016.1001

Cheng, H., Han, L. Y., Wu, Z. J., and Zhou, X. P. (2021). Experimental study on the whole failure process of anti-dip rock slopes subjected to external loading. *Bull. Eng. Geol. Environ.* 80 (8), 6597–6613. doi:10.1007/s10064-021-02311-5

Ding, B. D., Han, Z. Y., Zhang, G. C., Beng, X. T., and Yang, Y. C. (2021). Flexural toppling mechanism and stability analysis of an anti-dip rock slope. *Rock Mech. Rock Eng.* 54 (8), 3721–3735. doi:10.1007/s00603-021-02435-w

Dong, M. L., Zhang, F. M., Lv, J. Q., Fei, Y., and Li, Z. N. (2020). Study of stability influencing factors of excavated anti-dip rock slope. *Ksce J. Civ. Eng.* 24 (8), 2293–2303. doi:10.1007/s12205-020-1412-4

Dong, M. L., Zhang, F. M., Yu, C., Lv, J. Q., Zhou, H. X., Li, Y. K., et al. (2022). Influence of a dominant fault on the deformation and failure mode of anti-dip layered rock slopes. *Ksce J. Civ. Eng.* 26 (8), 3430–3439. doi:10.1007/s12205-022-1852-0

Gao, L. T., Yan, E. C., and Xie, L. F. (2015). Improved goodman-bray method in consideration of groundwater effect. *J. Yangtze River Sci. Res. Inst.* 32 (2), 78–83. doi:10.3969/j.issn.1001-5485.2015.02.017

Goodman, R. E., and Bray, J. W. (1976). Toppling of rock slopes, specialty conference on rock engineering for foundations and slopes. *Am. Soc. Civ. Eng.* 2, 201–234.

Gschwind, S., Loew, S., and Wolter, A. (2019). Multi-stage structural and kinematic analysis of a retrogressive rock slope instability complex (Preonzo, Switzerland). *Eng. Geol.* 252, 27–42. doi:10.1016/j.enggeo.2019.02.018

He, M. C., Sui, Q. R., Li, M. N., Wang, Z. J., and Tao, Z. G. (2022). Compensation excavation method control for large deformation disaster of mountain soft rock tunnel. *Int. J. Min. Sci. Technol.* 32 (5), 951–963. doi:10.1016/j.ijmst.2022.08.004

Huang, R. Q. (2012). Mechanisms of large-scale landslides in China. *Bull. Eng. Geol. Environ.* 71 (1), 161–170. doi:10.1007/s10064-011-0403-6

Jiang, X. N., Fan, L. G., Zhou, Y. L., and Zhu, T. Y. (2016). Research on the deformation failure mechanism and influence factors of large dipping steeply anti-dip rock landslide. *Chin. J. Undergr. Space Eng.* 12 (2), 356–361.

Lei, Z. D., Wu, B. S., Wu, S. S., Nie, Y. X., Cheng, S. Y., and Zhang, C. Y. (2022). A material point-finite element (MPM-FEM) model for simulating three-dimensional soil-structure interactions with the hybrid contact method. *Comput. Geotechnics* 152, 105009. doi:10.1016/j.compgeo.2022.105009

Li, L. Q., Ju, N. P., Zhang, S., Deng, X. X., and Sheng, D. C. (2019). Seismic wave propagation characteristic and its effects on the failure of steep jointed anti-dip rock slope. *Landslides* 16 (1), 105–123. doi:10.1007/s10346-018-1071-4

Liang, X., Tang, S. B., Tang, C. A., Hu, L. H., and Chen, F. (2022). Influence of water on the mechanical properties and failure behaviors of sandstone under triaxial compression. *Rock Mech. Rock Eng.* 56, 1131–1162. doi:10.1007/s00603-022-03121-1

Liu, C. H., Jaksa, M. B., and Meyers, A. G. (2009). A transfer coefficient method for rock slope toppling. *Can. Geotechnical J.* 46 (1), 1–9. doi:10.1139/t08-094

Liu, C. H., Jaksa, M. B., and Meyers, A. G. (2010). Toppling mechanisms of rock slopes considering stabilization from the underlying rock mass. *Int. J. Rock Mech. Min. Sci.* 47 (2), 348–354. doi:10.1016/j.ijrmms.2009.11.008

Martino, S., Cercato, M., Della Seta, M., Esposito, C., Hailemikael, S., Iannucci, R., et al. (2020). Relevance of rock slope deformations in local seismic response and microzonation: Insights from the Accumoli case-study (central Apennines, Italy). *Eng. Geol.* 266, 105427. doi:10.1016/j.enggeo.2019.105427

Nie, W., Wang, W. Q., Tao, Z. G., Zhu, C., and Chen, Y. (2022). Numerical modeling of the NPR-cable and its applications for analysis of a slide-toe-toppling failure. *Comput. Geotechnics* 149, 104852. doi:10.1016/j.compgeo.2022.104852

Ning, Y. B., Zhang, G. C., Tang, H. M., Shen, W. C., and Shen, P. W. (2019). Process analysis of toppling failure on anti-dip rock slopes under seismic load in southwest China. *Rock Mech. Rock Eng.* 52 (11), 4439–4455. doi:10.1007/s00603-019-01855-z

Ren, D. Z., Wang, X. Z., Kou, Z. H., Wang, S. C., Wang, H., Wang, X. G., et al. (2023). Feasibility evaluation of CO2 eor and storage in tight oil reservoirs: A demonstration project in the ordos basin. *Fuel* 331, 125652. doi:10.1016/j.fuel.2022.125652

Ren, Z. H., Chen, C. X., Sun, C. Y., and Wang, Y. (2022). Dynamic analysis of the seismo-dynamic response of anti-dip bedding rock slopes using a three-dimensional discrete-element method. *Appl. Sciences-Basel* 12 (9), 4640. doi:10.3390/app12094640

Shen, Q., Chen, C. X., Lu, H. F., and Zhao, Y. Y. (2010). Experimental research on the rheology characterisic of the red soft rock of badong group. *Disaster Adv.* 3 (4), 210–213. doi:10.1155/2021/6615379

Tang, S. B., Li, J. M., Ding, S., and Zhang, L. T. (2022). The influence of water-stress loading sequences on the creep behavior of granite. *Bull. Eng. Geol. Environ.* 81 (11), 482. doi:10.1007/s10064-022-02987-3

Tao, Z. G., Geng, Q., Zhu, C., He, M. C., Cai, H., Pang, S. H., et al. (2019). The mechanical mechanisms of large-scale toppling failure for counter-inclined rock slopes. *J. Geophys. Eng.* 16 (3), 541–558. doi:10.1093/jge/gxz020

Wang, G. J., Tian, S., Hu, B., Kong, X. Y., and Chen, J. (2020a). An experimental study on tailings deposition characteristics and variation of tailings dam saturation line. *Geomechanics Eng.* 23 (1), 85–92. doi:10.12989/gae.2020.23.1.085

Wang, G. J., Zhao, B., Wu, B. S., Wang, M. L., Liu, W. L., Zhou, H. M., et al. (2022a). Research on the macro-mesoscopic response mechanism of multisphere approximated heteromorphic tailing particles. *Lithosphere* 2022 (10), 1977890. doi:10.2113/2022/1977890

Wang, G. J., Zhao, B., Wu, B. S., Zhang, C., and Liu, W. L. (2023). Intelligent prediction of slope stability based on visual exploratory data analysis of 77 *in situ* cases. *Int. J. Min. Sci. Technol.* 33 (1), 47–59. doi:10.1016/j.ijmst.2022.07.002

Wang, H., Li, H., Tang, L., Ren, X., Meng, Q., and Zhu, C. (2022b). Fracture of two three-dimensional parallel internal cracks in brittle solid under ultrasonic fracturing. *J. Rock Mech. Geotechnical Eng.* 14 (3), 757–769. doi:10.1016/j.jrmge.2021.11.002

Wang, Q., Xu, S., Xin, Z. X., He, M. C., Wei, H. Y., and Jiang, B. (2022c). Mechanical properties and field application of constant resistance energy-absorbing anchor cable. *Tunn. Undergr. Space Technol.* 125, 104526. doi:10.1016/j.tust.2022.104526

Wang, Z. Y., Gu, D. M., and Zhang, W. G. (2020b). Influence of excavation schemes on slope stability: A DEM study. *J. Mt. Sci.* 17 (6), 1509–1522. doi:10.1007/s11629-019-5605-6

Wei, M. H. (2015). Anti-dip layered slope deformation and failure mode of formation thickness and other properties. *Sci. 'Technology Eng.* 15 (31), 141–146. doi:10.3969/j.issn.1671-1815.2015.31.026

Weng, M. C., Chang, C. Y., Jeng, F. S., and Li, H. H. (2020). Evaluating the stability of anti-dip slate slope using an innovative failure criterion for foliation. *Eng. Geol.* 275, 105737. doi:10.1016/j.enggeo.2020.105737

Wu, S. S., Zhao, G. F., and Wu, B. S. (2022). Real-time prediction of the mechanical behavior of suction caisson during installation process using GA-BP neural network. *Eng. Appl. Artif. Intell.* 116, 105475. doi:10.1016/j.engappai.2022.105475

Xie, L. F., Zhu, Q. Y., Qin, Y. J., Wang, J. H., and Qian, J. G. (2020). Study on evolutionary characteristics of toppling deformation of anti-dip Bank Slope based on energy field. *Sustainability* 12 (18), 7544. doi:10.3390/su12187544

Xu, W. J., Wang, L., and Cheng, K. (2022). The failure and river blocking mechanism of large-scale anti-dip rock landslide induced by earthquake. *Rock Mech. Rock Eng.* 55 (8), 4941–4961. doi:10.1007/s00603-022-02903-x

Zheng, Z., Su, G. S., Jiang, Q., Pan, P. Z., Huang, X. H., and Jiang, J. Q. (2022). Mechanical behavior and failure mechanisms of cylindrical and prismatic rock specimens under various confining stresses. *Int. J. Damage Mech.* 31 (6), 864–881. doi:10.1177/10567895221083997

Zhu, C., He, M. C., Karakus, M., Cui, X. B., and Tao, Z. G. (2020). Investigating toppling failure mechanism of anti-dip layered slope due to excavation by physical modelling. *Rock Mech. Rock Eng.* 53 (11), 5029–5050. doi:10.1007/s00603-020-02207-y